Materials Transactions, Vol. 44, No. 10 (2003) pp. 1919 to 1925
Special Issue on Nano-Hetero Structures in Advanced Metallic Materials

OVERVIEW

Development of Nanostructures in Metallic Materials with Low Stacking Fault Energies During Surface Mechanical Attrition Treatment (SMAT)

Nairong Tao[1], Hongwang Zhang[1,2], Jian Lu[3] and Ke Lu[1]*

[1]*Shenyang National Laboratory for Materials Science, Institute of Metal Research, Chinese Academy of Sciences, Shenyang 110016, P.R China*
[2]*Institute of Materials & Technology, Dalian Maritime University, Dalian 116026, P.R China*
[3]*LASMIS, University of Technology of Troyes, 10000, Troyes, France*

Surface mechanical attrition treatment (SMAT) technique was developed to synthesize a nanostructured surface layer on metallic materials for upgrading their overall properties and performance. In this paper, the grain refinement process during SMAT was investigated in materials with low stacking fault energies (SFE, Inconel 600 alloy and AISI 304 stainless steel) by means of transmission electron microscopy and high-resolution electron microscopy, respectively. Grain subdivision was performed by the interaction of mechanical microtwins with dislocations in Inconel 600. For AISI 304 stainless steel with a lower SFE, twin-twin intersections subdivide initial grains into refined blocks with sizes ranging from nanometers to submicrometers. Such grain subdivision processes of the interaction of microtwins with dislocations or microtwins obviously differ from those observed in the high SFE materials in which dislocation interactions predominate the grain refinement.

(Received April 25, 2003; Accepted May 15, 2003)

Keywords: *nanostructured materials, surface mechanical attrition treatment, grain refinement, mechanical twin*

1. Introduction

Most failures of materials occur on their surfaces, such as fatigue fracture, fretting fatigue, wear and corrosion etc., which are very sensitive to the structure and properties of the material surface. Optimization of the surface microstructure and properties may effectively enhance the global behavior and service lifetime of materials. Increasing evidences have been detected for novel properties of nanocrystalline materials, including high hardness and strength,[1–3] enhanced physical properties,[1–3] rapid atomic diffusion,[4] improved tribological properties,[5] and superplasticity at low temperatures,[6,7] *etc.* Hence, surface modification by generation of a nanostructured surface layer on a material, or referred as surface nanocrystallization (SNC), would be expected to improve the global properties and performance of materials.

Recently, a surface mechanical attrition treatment (SMAT) technique was developed for realizing SNC in metallic materials.[8,9] Owing to the severe plastic deformation in the surface layer induced by the mechanical attrition, the coarse-grained structure at the surface is refined into the nanostructures without changing the overall chemical compositions. The SMAT has been successfully applied in many metallic material systems including pure metals, steels, and alloys,[9–14] on which a nanostructured surface layer with thicknesses of 10-50 μm has been obtained. Obvious enhancement in the mechanical and tribological properties of the materials is observed after SMAT.[11,15] In addition, surface nitriding kinetics of iron was found to be greatly enhanced by the SMAT process.[4]

Understanding the underlying mechanism for formation of nanostructures during SMAT is crutial. Owing to the gradient variation of the strain and strain rate from the treated top surface (both are very large) to the deep matrix (essentially zero), the structure evolution process during SMAT may signed by the microstructure characteristics (with different strains) at different depths so that the surface layer of a SMAT sample with different levels of strain and strain rate provides a unique opportunity to examine the grain refinement process.

Analogous to the grain refinement mechanism during plastic deformation of bulk metals, formation of nanostructures from the coarse-grained polycrystals in the surface layer upon the SMAT involves various dislocation activities and development of grain boundaries. So far, our investigations showed that the grain refinement via SMAT resulted from various dislocation activities in metals and alloys with medium to high staking fault energies (SFEs).[12,13] Straining-induced dislocations arrange themselves into various dislocation configurations depending upon the nature of deformed materials, such as dense dislocation walls in specific slip planes, dislocation tangles, dislocation cells. Interactions of these dislocations lead to development of subgrain boundaries across which small misorientations are induced. With further straining, subgrain boundaries evolve into high-angle grain boundaries that subdivide the original grains into refined structures. This grain refinement mechanism has also been found in metals and alloys with medium to high SFE deformed via other deformation routes.[16,17]

For materials with low SFEs, plastic deformation mode may change from dislocation slip to mechanical twinning. Nevertheless, investigation on the strain-induced grain refinement process in low SFE materials is still lacking, especially when deformed at high strain rates. In this work, an Inconel 600 alloy and an AISI 304 stainless steel (both have low SFEs) were chosen to investigate the strain-induced grain refinement during the SMAT process.

2. Experimental

The materials used in this work are an Inconel 600 alloy with chemical compositions of (in mass%): 15.5 Cr, 8 Fe, 0.1

*Corresponding author: E-mail address: lu@imr.ac.cn

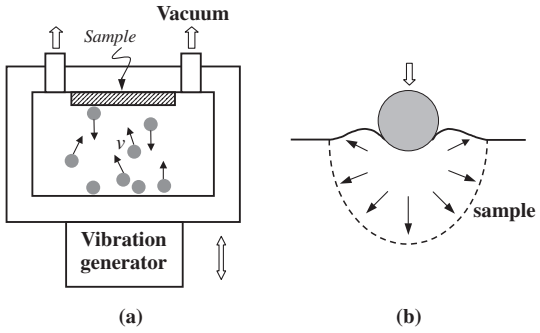

Fig. 1 Schematic illustrations of the SMAT set-up (a) and the localized plastic deformation in the surface layer by the impacting of the shot (b).

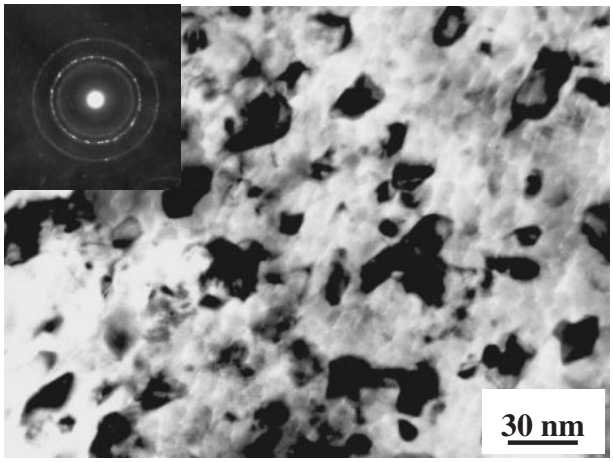

Fig. 2 TEM image showing nanocrystallites in the top surface of the SMAT Inconel 600 sample.

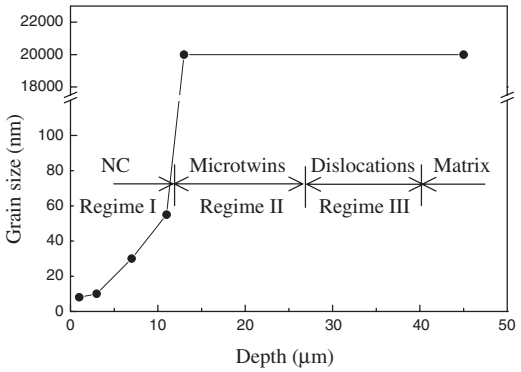

Fig. 3 Variation of grain size with the depth from the top surface for the SMAT Inconel 600 sample (NC presents nanocrystallites).

C, 0.8 Mn, 0.38 Si, 0.4 Cu with the balance Ni, and an AISI 304 stainless steel with chemical compositions of (in mass%): 0.049C, 18.20Cr, 8.66Ni, 0.58Si, 1.04Mn, 0.021P, 0.007S and balance Fe. Before SMAT, the samples were annealed for diminishing the effect of mechanical processing and obtaining homogeneous coarse grains.

Figure 1(a) shows a schematic illustration of the SMAT set-up used in the present work.[18] Spherical steel balls with smooth surface are placed in a reflecting chamber that is vibrated by a vibration generator with vibration frequency ranging from 50 to 20 kHz. When the balls are resonated, the sample surface to be treated is impacted by a large number of flying balls over a short period of time. Each impact will induce plastic deformation with a high strain rate in the sample surface, as schematically shown in Fig. 1(b). The impact directions are random due to the random flying directions of the balls inside the vibration chamber. As a consequence, the repeated multidirectional impacts at high strain rates onto the sample surface result in severe plastic deformation in the surface layer. In this work, Inconel 600 was treated for 12 min with a vibration frequency of 20 kHz and steel balls of 3 mm in diameter. A vibration frequency of 50 Hz and steel balls with a diameter of 8 mm were selected to process AISI 304 stainless steel for 15 min.

Microstructure features of the surface layer in the SMAT samples were characterized by using a Philip EM-420 transmission electron microscope (TEM, operating at a voltage of 120 kV) and a JEOL-2010 high-resolution electron microscope (HREM, at 200 kV), respectively. The preparation procedures of cross-sectional thin foil samples for TEM observations have been described in detail in.[12,14]

3. Results

In order to understand the grain refinement mechanism of materials during SMAT, a systematic investigation on the microstructure in the surface layer with different levels of straining is crucial. Systematical cross-sectional TEM observations were carried out on the SMAT samples of Inconel 600 and AISI 304 stainless steel samples, respectively.

3.1 Inconel 600

Figure 2 shows a typical TEM image of the top surface layer (about 4 μm deep) in the SMAT Inconel 600 sample. The microstructure is characterized by nanometer-sized crystallites with random crystallographic orientations, as indicated by the selected area electron diffraction (SAED) pattern. The grain size is in a range of 10-30 nm. Clearly, a nanostructured surface layer was developed in the Inconel 600 sample during SMAT.

Cross-sectional TEM observations in the SMAT Inconel 600 sample showed various types of microstructures in the surface layer, including randomly-oriented equiaxed nanocrystallites, mechanical microtwins and planar dislocation arrays with the depth increasing, as shown in Fig. 3. Note that the size of nanocrystallites increases as the depth increases in the top layer of 12 μm thick. Adjacent to the nanostructured surface layer, the prominent feature of microstructure is mechanical microtwins instead of submicro- and micrometer-sized subgrains or dislocation cells as observed in SMAT Fe and Al-based alloy with high SFEs. Planar dislocation arrays are found in plastic deformation regime adjacent to the strain-free matrix. Such microstructures differ from that of the SMAT Fe and Al-based alloy samples in which the grain (or dislocation cell) size gradually increases from nanometer to micrometer with the depth increasing.[12,13]

In the low strain and strain rate region (Regime III in Fig. 3), microstructures are characterized by planar dislocation arrays and grids formed in {111} slip planes with negligible cross-slip. Figure 4 shows a typical TEM image in this regime. In grain 1 and grain 2, strain-induced disloca-

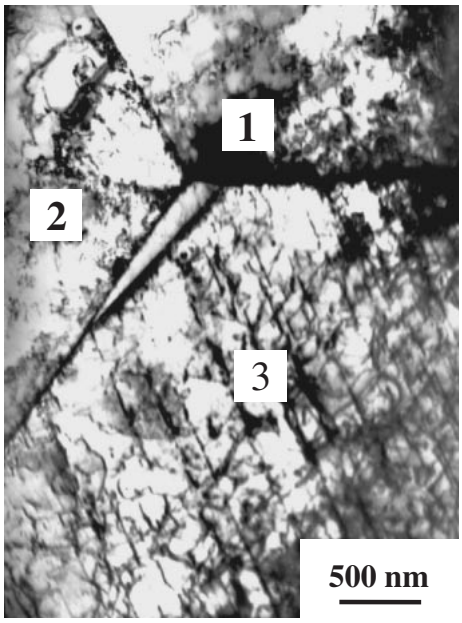

Fig. 4 A cross-sectional TEM image showing the dislocation structures in the Inconel 600 sample.

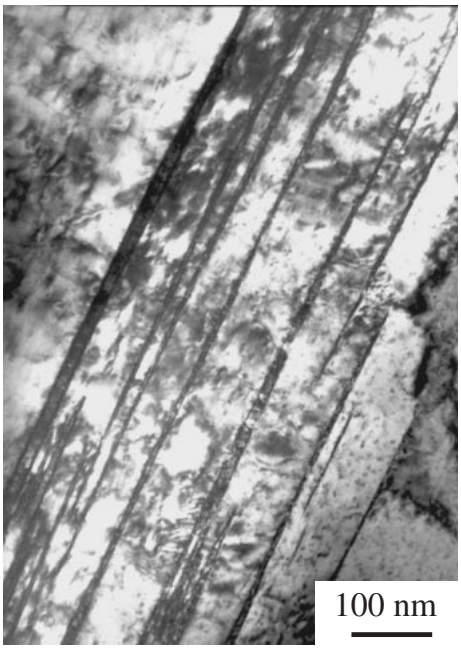

Fig. 5 A cross-sectional TEM image showing high-density mechanical microtwins in the Inconel 600 sample.

tions form planar dislocation arrays, and planar dislocation grids are observed in grain 3. The spacing between dislocation arrays varied from 100 nm to 1 μm, depending upon crystallographic orientations of original grains and the level of plastic strain. As the depth from the top surface decreased, planar dislocation grids became denser and the spacing between dislocation arrays reduced.

The deformation mode changes from slip to mechanical twinning as the strain increases (Regime II in Fig. 3). Mechanical twins may initiate from different regions of the original coarse grains and terminate at the interior of grains, or at the boundaries of their conjugated microtwins. No twin-twin intersections were found in the sample. Figure 5 shows a TEM image of high-density mechanical microtwins in regime II. These microtwins are of $\{111\}\langle 112\rangle$ type and are parallel to each other. The thickness of mechanical microtwins observed in the surface layer is in the range of nanometer, usually as small as a few nanometers. Development of high-density mechanical microtwins leads to reduction of the thickness of corresponding matrix down to the nanometer scale, as seen in Fig. 5. Apparently, formation of high-density microtwins introduced a large amount of twin boundaries that subdivide the original coarse grains into lamellar twin-matrix alternate blocks (LTMABs), *i.e.*, lamellar nanocrystallites with special crystallographic orientations.

High-density dislocations were also observed inside LTMABs. The dislocations inside LTMABs will arrange themselves into dislocation walls to accommodate further plastic deformation. Figure 6 is a HREM image showing typical arrangements of dislocation walls observed inside a microtwin. Some dislocations form a dislocation wall across the thickness of the microtwin, as indicated by (I) in Fig. 6. This dislocation wall seems to "cut" through thickness of the microtwin lamellae. Another pattern of dislocation walls is characterized by aggregation of several dislocation pairs with

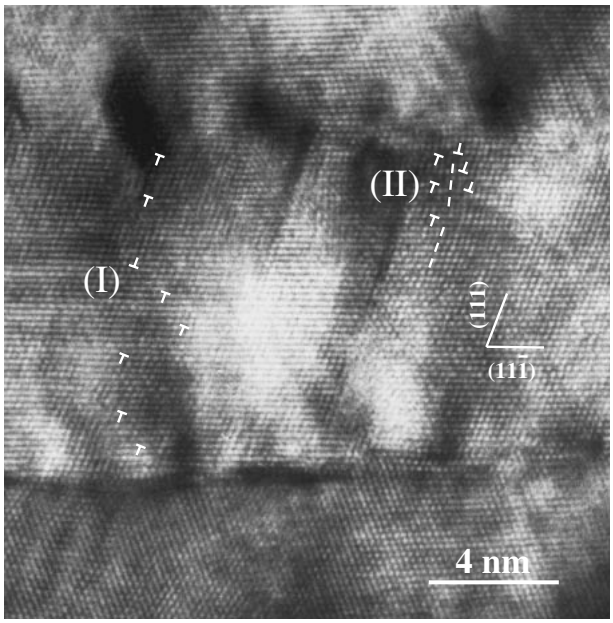

Fig. 6 Typical arrangements of dislocation walls in the Inconel 600 sample: dislocation walls across the thickness of the microtwin (I) and dislocation multipole walls (II) subdividing mechanical microtwins into equiaxed nanometer-sized blocks with misorientations.

opposite Burgers vectors forming dislocation multipole walls in a very small region, as labeled (II) in Fig. 6. These dislocations are so arranged that a tiny (nanometer-sized) block is surrounded by the dislocations and an apparent misorientation exists across the dislocation multipole walls. For example, the dislocation multipole walls (II) in Fig. 6 induced a misorientation angle of about 16° across the nanometer-sized block and the surrounding lattice. In fact, these two types of dislocation walls were frequently observed inside both the microtwin and the matrix lamellae. With an

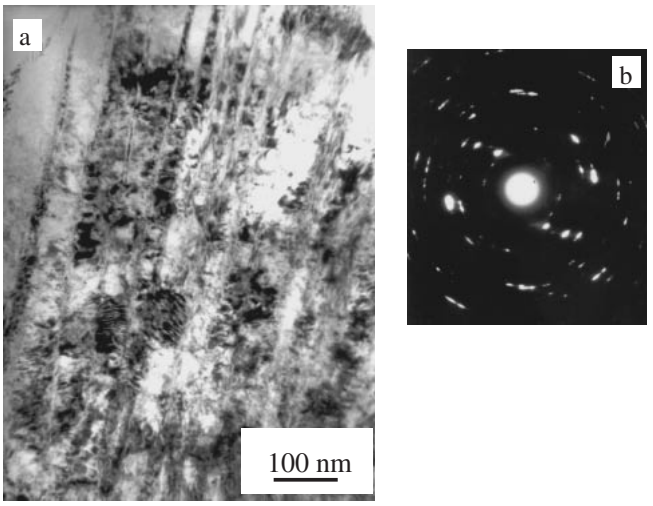

Fig. 7 (a) A typical microstructure of microtwin and (b) the corresponding SAED for the Inconel 600 sample.

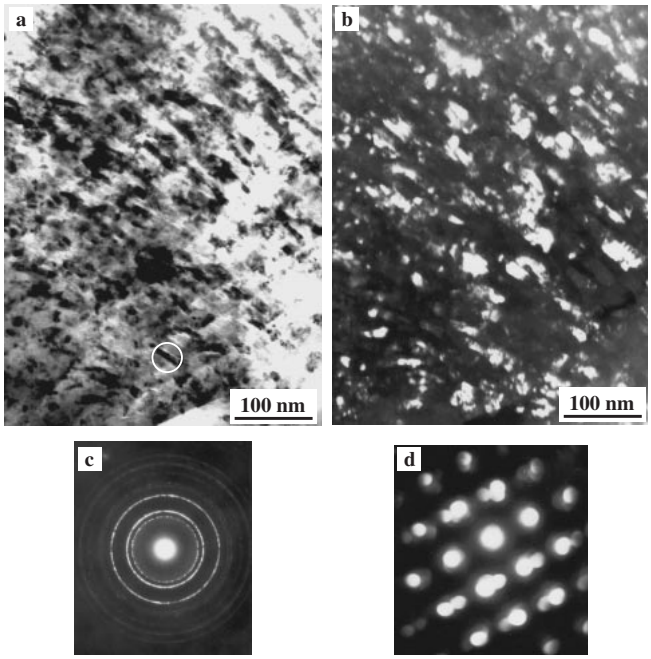

Fig. 8 (a) Bright-field; (b) dark-field TEM images in SMAT Inconel 600 showing the nanocrystallites derived from mechanical microtwins in the top surface layer of the Inconel 600 sample; (c) the corresponding SAED and (d) the micro-area electron diffraction patterns of the outlined region with a circle in (a).

increasing straining, more dislocations are generated to form more dislocation walls that subdivide LTMABs.

Figure 7 is a typical microstructure showing break-ups of LTMABs into equiaxed nanostructures with misorientations at a smaller depth from the surface. Inside LTMABs, some nanometer-sized blocks with distinct contrast from the surroundings result from the constant increase in misorientations of the nanometer-sized blocks surrounded by dislocation walls (as in Fig. 6). The corresponding SAED pattern indicated that some randomly-oriented nanocrystallites have been formed in the LTMABs.

Figure 8 is typical TEM image showing the evolution of mechanical microtwins into randomly orientated nanocrytallites. In Fig. 8, it is found that the nanocrystallites were roughly equiaxed and separated with large-angle boundaries, as indicated by the continuous diffraction rings in the corresponding SAED pattern (Fig. 8(c)). From the bright and dark field images, it is interesting to note that the nanocrystallites seem to be arranged in parallel bands. Further noted that these adjacent parallel bands possessed imperfect fcc twin relations, which was indicated by the micro-area electron diffraction patterns, as seen in Fig. 8(d). No experimental results showed that two adjacent nanostructured blocks along any parallel band (*i.e.*, in one microtwin) possess twin relations, indicating that the refined blocks are not derived from twin-twin intersections. The results described above clearly indicate that randomly orientated nanocrytallites in the top surface layer are derived from the nanometer-sized blocks within LTMABs via formation of large-angle grain boundaries across these blocks. The interactions of mechanical microtwins with dislocations dominate the grain subdivision process.

3.2 AISI 304 stainless steel

Equiaxed randomly-oriented nanocrystallites were obtained in the surface layer of the SMAT AISI 304 sample.[14] Figure 9 shows a typical plane-view TEM micrograph and the statistic grain size distribution for the top surface. The microstructure (Fig. 9(a)) is characterized by uniformly-distributed nanometer-scale grains. The corresponding SAED pattern shows that these grains are martensites with random orientations, and no austenite is detected. The histogram of grain size distribution obtained from the dark field images is characterized by a normal logarithmic distribution with a narrow size distribution of 8-50 nm. The average grain size is approximately 10 nm. Differing from Inconel 600, the size of grains (or blocks) gradually increases from nanometer to submicrometer with the depth increasing in the surface layer of the AISI 304 sample. The submicro-sized grains consist of both martensite and austenite, and their orientations are less random.

In the regime adjacent to the strain-free matrix, the microstructure of the SMAT AISI 304 sample is characterized by planar dislocation arrays and stacking faults. The planar dislocation arrays in two directions intersect with each other with an angle of about 70.5° (the angle between two {111} crystallographic planes), forming dislocation grids. The spacing between dislocation arrays depends upon the orientation of original grains, ranging from 200 nm to 1 μm.

As strain increases, plastic deformation is accommodated by mechanical twins. Compared with the Inconel 600 sample, the prominent feature is that twin-twin intersections were observed in the AISI 304 sample. Figure 10 shows a typical microstructure of twin-twin intersections in the surface layer. Note that the intersections of mechanical twins subdivide the original austenite grains into refined blocks. Figure 11 is TEM bright and dark images showing the formation of regular-shaped blocks (submicron-sized) with straight boundaries. It is obvious that the formation of rhombic blocks results from intersections of mechanical twins. The corresponding SAED pattern shows that some of these blocks are of b.c.c. martensite phase. It indicates that the martensite

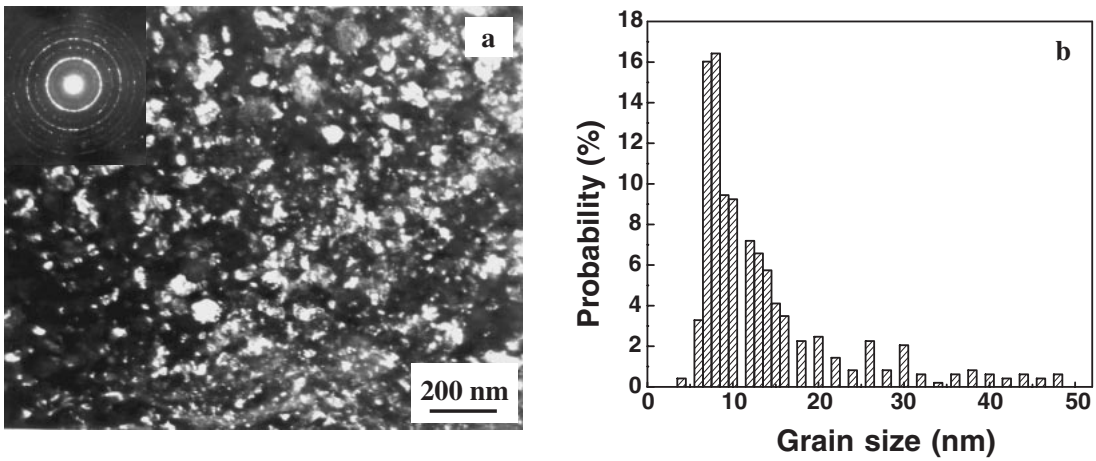

Fig. 9 (a) Typical plane-view TEM observations and (b) the statistic grain size distribution of the top surface in the AISI 304 sample.

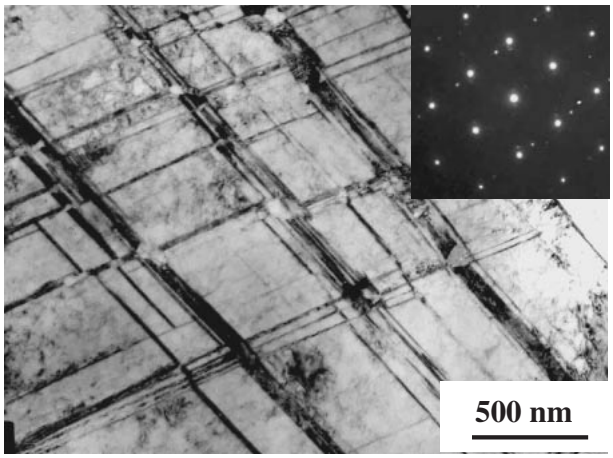

Fig. 10 Cross-sectional TEM image of the microstructure at the depth of about 150 μm in the AISI 304 sample.

phase forms at intersections of two sets of mechanical twins, analogy to that observed in the AISI 304 stainless steel during the shock deformation[19] and balanced biaxial straining.[20] The size of martensite is dependent upon the thickess of twins operated, thinner mechanical twins may result in finer martensite, and here typical submicron-sized martensites are identified as indicated by the arrows.

With a further increasing of strain, nanometer-sized blocks are formed due to the intersections of nanometer-thick mechanical twins. A martensite transformation occurred in the refined blocks formed by intersecting of twins, analogy to those observed in Fig. 10, but the size of the blocks is much smaller. The shapes of the nanometer-sized blocks become less regular.

4. Discussion

Based on the microstructure characteristics from the top surface to the strain-free matrix, formation mechanisms of nanocrystallites in the SMAT samples of Inconel 600 and AISI 304 were proposed. The basic processes of grain refinement can be schematically illustrated in Fig. 12, in which every process will be discussed in terms of experimental observations.

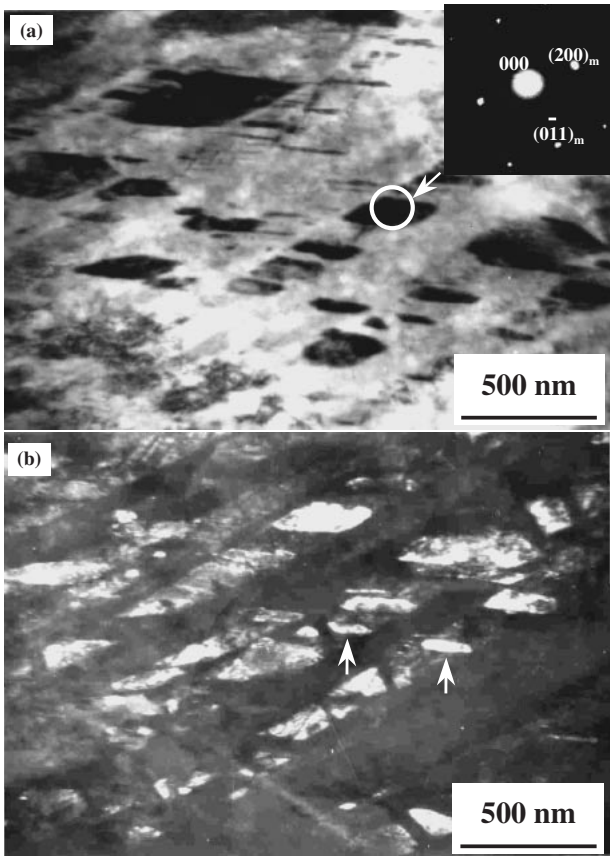

Fig. 11 (a) A bright-field and (b) dark-field cross-sectional TEM images at the depth of about 100 μm in the AISI 304 sample.

4.1 Formation of planar dislocation arrays and mechanical twins

In low strain and strain rate regime, the strain-induced dislocations in Inconel 600 and the austenite phase (fcc) of AISI 304 slip mainly on their respective {111} planes, forming planar dislocation arrays and grids, instead of irregular dislocation cells (as in fcc Al-alloy), or dense dislocation walls (as in bcc Fe). Planar dislocation arrays and grids are typical dislocation configurations observed in f.c.c. metals and alloys with low SFEs when deformed at low strains and strain rates. This configuration can be attributed to

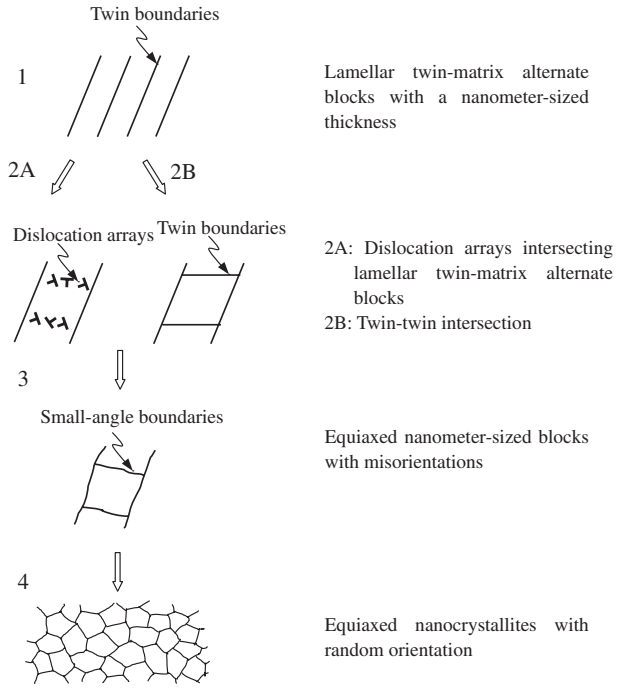

Fig. 12 A schematic illustration of grain refinement during SMAT for the two samples with low stacking fault energies.

the low SFE that makes it difficult for partial dislocations to cross-slip and causes dislocations to arrange themselves into planar arrays on their primary slip planes.

Generally, slip dominates the deformation process in a wide range of plastically deformed materials with medium-high SFE values. However, the critical shear stress for twinning decreases with a reduction of SFE value, *i.e.* materials with a low SFE favor mechanical twinning, especially at high strain rates and/or at low temperatures. For Inconel 600 and AISI 304, the SMAT process may provide preferable conditions for development of mechanical microtwins due to the low deformation temperature (close to ambient temperature) and high strain rates that lead to suppression of thermally activated dislocation processes. This resulted in stresses high enough to nucleate and grow mechanical microtwins by the formation of stacking faults. Formation of a high density of ultra-thin (in the nanometer scale) mechanical twins implies the surface layer undergone plastic deformation at a very high strain rate (estimated to be about 10^3–$10^4\ s^{-1}$) without much temperature rise during the SMAT process. For the Inconel 600 and AISI 304 samples, the development of the nanometer-thick twins plays an important role in grain subdivisions and formation of nanocrystallites in the surface layer.

4.2 Grain subdivision

A twin boundary is a particularly simple case of periodic boundary or a "special" large-angle boundary with a very high degree of coincidence. Formation of high-density parallel twins with a single direction in the Inconel 600 and AISI 304 samples introduced a large amount of twin boundaries to subdivide the original coarse grains into LTMABs (Step 1in Fig. 12).

4.2.1 Dislocation walls subdividing LTMABs in Inconel 600

It was found that all microtwins in Inconel 600 terminate at the interior of grains or at the boundaries of their conjugated microtwins. This means that the driving force for growth of microtwins is not so high to overcome the barriers of the encountered microtwin boundary. With strain increasing, dislocation activities become functional inside LTMABs for accommodating further plastic deformation when formation of mechanical microtwins becomes more difficult within the thin lamellae. For minimizing the strain energy, dislocations in the thin twin-matrix lamellae arrange themselves into dislocation walls (Step 2A). As strain further increases, formation of subboundaries originating from the dislocation walls subdivides LTMABs into equiaxed nanometer-sized blocks with misorientations (Step 3).

4.2.2 Twin-twin intersections subdividing LTMABs in AISI 304

For the materials with even smaller SFEs, the driving force for growth of mechanical twins is possibly large enough to overcome the barriers of the encountered microtwin boundary so that intersection of twins are feasible. In the AISI 304 sample with a SFE as small as $16.8\ mJ/m^2$, twin-twin intersections were observed to form rhombic blocks (Fig. 10). Therefore, twin-twin intersections in AISI 304 could subdivide the initial coarse grains into rhombic blocks with changed orientations and bordered by large-angle boundaries (Step 2B and 3 in Fig. 12). These boundaries are quite different from the dislocation boundaries developed in other plastic deformed materials with medium-high SFEs.[21] They are large-angle boundaries ($\Sigma 3$ and $\Sigma 9$ etc) when formed, differing from dislocation boundaries that increase their boundary misorientations through accumulation and annihilation of more dislocations at grain boundaries.

For AISI 304, twin-twin intersections could not only subdivide the original grains efficiently through introducing different boundaries ($\Sigma 3$, $\Sigma 9$, and other boundaries), but also induce a martensite transformation (introducing phase boundaries) leading to formation of refined microstructures.

4.3 Formation of randomly oriented nanocrystallites

Formation of randomly orientated nanocrystallites requires a substantial variation in the related orientations of these nanometer-sized blocks (Step 4 in Fig. 12). Possible mechanisms responsible for the formation of random orientations may involve in grain boundary sliding and/or grain rotation. When the grain size is reduced down to the nanometer range, the grain rotation and grain boundary sliding will be much easier with respect to the coarse ones.[22] Grain rotation is an alternative process accommodating plastic deformation of nanocrystallites, which may effectively increase the misorientations and result in the formation of randomly orientated nanocrystallites.[23]

In the AISI 304 sample, the martensite phase forms at twin intersections, of which the size ranges from several manometers to submicrometers. Such a phase transformation is a unique process that facilitates the grain refinement procedure as well.

5. Summary

The microstructures in the surface layer of an Inconel 600 and an AISI 304 stainless steel were refined into randomly orientated nanocrystallites by means of SMAT at room temperature. Grain subdivision was performed by the interaction of mechanical microtwins with dislocations in Inconel 600. For AISI 304 stainless steel with an even lower SFE, twin-twin intersections subdivide initial grains into refined blocks with sizes ranging from nanometers to submicrometers. Such grain subdivision processes of the interaction of microtwins with dislocations or microtwins obviously differ from those observed in other materials (dislocation interactions) reported in the literature. This indicates that the strain-induced grain refinement mechanism is sensitive to the nature of materials and the deformation conditions.

Acknowledgments

Financial support from the National Science Foundation of China, the Ministry of Science and Technology of China (Grant G1999064505), Framatome corporation of France and Ministry of Research of France (Grant 2001882, CPER EN2040) is acknowledged.

REFERENCES

1) H. Gleiter: Prog. Mater. Sci. **33** (1988) 223-315.
2) C. Suryanarayana: Int. Mater. Rev. **40** (1995) 41-64.
3) K. Lu: Mater. Sci. Eng. **R16** (1996) 161-221.
4) W. P. Tong, N. R. Tao, Z. B. Wang, J. Lu and K. Lu: Science **299** (2003) 686-688.
5) D. G. Morris: *Mechanical Behaviour of Nanostructured Materials*, (Trans. Tech. Publications Ltd., Switzerland, 1998) pp. 70-72.
6) S. X. McFadden, R. S. Mishra, R. Z. Valiev, A. P. Zhilyaev and A. K. Mukherjee: Nature **298** (1999) 684-686.
7) L. Lu, M. L. Sui and K. Lu: Science **287** (2000) 1463-1466.
8) K. Lu and J. Lu: J. Mater. Sci. Technol. **15** (1999) 193-197.
9) N. R. Tao, M. L. Sui, J. Lu and K. Lu: Nanostruct. Mater. **11** (1999) 433-440.
10) G. Liu, J. Lu and K. Lu: Mater. Sci. Eng. A**286** (2000) 91-95.
11) G. Liu, S. C. Wang, X. F. Lou, J. Lu and K. Lu: Scr. Mater. **44** (2001) 1791-1795.
12) N. R. Tao, Z. B. Wang, W. P. Tong, M. L. Sui, J. Lu and K. Lu: Acta Mater. **50** (2002) 4603-4616.
13) X. Wu, N. Tao, Y. Hong, B. Xu, J. Lu and K. Lu: Acta Mater. **50** (2002) 2075-2084.
14) H. W. Zhang, Z. K. Hei, G. Liu, J. Lu and K. Lu: Acta mater, **51** (2003) 1871-1881.
15) Z. B. Wang, N. R. Tao, S. Li, W. Wang, G. Liu, J. Lu and K. Lu: Mater. Sci. Eng. A, (2003) in press.
16) A. Belyakov, T. Sakai, H. Miura and K. Tsuzaki: Philos Mag. A **81** (2001) 2629-2643.
17) B. Bay, N. Hansen, D. A. Hughes and D. Kuhlmann-wilsdorf: Acta Metall. **40** (1992) 205-219.
18) K. Lu and J. Lu: *Chinese Patent*, No. 01122980. 2 (2001); *French Patent*, FR2812284 (2001).
19) K. A. Johnson, L. E. Murr and K. P. Staudhammer: Acta Metall. **33** (1985) 677-684.
20) L. E. Murr, K. P. Staudhammer and S. S. Hecker: Metall. Trans. **13A** (1982) 627-635.
21) N. Hansen: Metall. Mater. Trans. **32A** (2001) 2917-2935.
22) H. Von Swygenhoven, D. Farkas and A. Caro: Phys. Rev. B **62** (2000) 831-838.
23) E. Hellstern, H. J. Fecht, Z. Fu and W. L. Johnson: J. Appl. Phys. **65** (1989) 305-310.